INTERFACE

rsif.royalsocietypublishing.org

Research

Cite this article: Lim Z, Smith DG, Kolanowski JL, Mattison RL, Knowles JC, Baek S-Y, Chrzanowski W, New EJ. 2018 A reversible fluorescent probe for monitoring Ag(I) ions. *J. R. Soc. Interface* **15**: 20180346.
http://dx.doi.org/10.1098/rsif.2018.0346

Received: 15 May 2018
Accepted: 22 June 2018

Subject Category:
Life Sciences–Chemistry interface

Subject Areas:
nanotechnology, chemical biology, biotechnology

Keywords:
silver, fluorescent probe, phosphate glass, antibacterial

Authors for correspondence:
Wojciech Chrzanowski
e-mail: wojciech.chrzanowski@sydney.edu.au
Elizabeth J. New
e-mail: elizabeth.new@sydney.edu.au

Electronic supplementary material is available online at https://dx.doi.org/10.6084/m9.figshare.c.4149821.

THE ROYAL SOCIETY PUBLISHING

A reversible fluorescent probe for monitoring Ag(I) ions

Zelong Lim[1], David G. Smith[1], Jacek L. Kolanowski[1], Rebecca L. Mattison[1], Jonathan C. Knowles[2,3,4], Song-Yi Baek[2], Wojciech Chrzanowski[5,6] and Elizabeth J. New[1,6]

[1]School of Chemistry, The University of Sydney, Sydney, New South Wales 2006, Australia
[2]Division of Biomaterials and Tissue Engineering, University College London Eastman Dental Institute, London WC1X 8LD, UK
[3]The Discoveries Centre for Regenerative and Precision Medicine, UCL Campus, London, UK
[4]Department of Nanobiomedical Science and BK21 Plus NBM Global Research Center for Regenerative Medicine, Dankook University, Cheonan, Korea
[5]The University of Sydney School of Pharmacy, Sydney, New South Wales 2006, Australia
[6]The University of Sydney Nano Institute, The University of Sydney, Sydney, New South Wales 2006, Australia

EJN, 0000-0002-2310-254X

Silver-containing nanomaterials are of interest for their antibiotic properties, for a wide range of applications from medicine to consumer products. However, much remains to be learnt about the degradation of such materials and their effects on human health. While most analyses involve measurement of total silver levels, it is important also to be able to measure concentrations of active free Ag(I) ions. We report here the preparation of a coumarin-based probe, thiocoumarin silver sensor 1 (**TcAg1**), that responds reversibly to the addition of silver ions through the appearance of a new fluorescence emission peak at 565 nm. Importantly, this peak is not observed in the presence of Hg(II), a common interferent in Ag(I) sensing. To establish the utility of this sensor, we prepared silver-doped phosphate glasses with demonstrated bactericidal properties, and observed the Ag(I) release from these glasses in solutions of different ionic strength. **TcAg1** is therefore a useful tool for the study of the environmental and medical effects of silver-containing materials.

1. Introduction

Silver is widely used in industrial applications due to its conductivity and malleability properties [1], as well as in medicine as an antibiotic coating and in wound treatment [2–5]. Because of its antibacterial properties, the use of silver coatings and nanoparticles is widespread in both the clinic and in everyday household items such as clothes, the lining of washing machines and refrigerators. In addition to their well-reported bactericidal properties [6,7], silver nanoparticles have also found application as imaging agents [8,9] and drug delivery vehicles [10,11]. The high toxicity of silver is crucial for the unique antibacterial properties of this metal, but there is concern about the effect of aquatic silver pollution on freshwater invertebrates [12] and fish [13]. The degradation products of silver nanoparticles in waterways are very different from those of elemental silver pollutants and there is therefore much interest in better understanding this speciation and its effects [14].

The apparent toxicity of silver is not directly correlated to total silver concentration, but is due primarily to the free Ag(I) ion itself [13,15]; environmental samples generally show lower toxicity of silver relative to laboratory standards with the same total concentration, due to the silver being bound or chelated to organic and inorganic ligands in the environmental samples [16–18]. In terms of silver nanoparticles and their use in medicine, Ag(I) release is the primary reason for bacterial toxicity; nanoparticle size

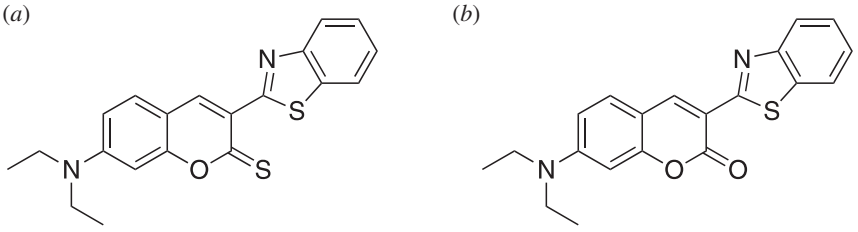

Figure 1. (*a*) Structure of thiocoumarin **TcAg1**; (*b*) structure of coumarin derivative after desulfurization (coumarin 6).

and morphology indirectly influence toxicity, mostly by modulating the release of Ag(I) [19]. In the chloride-rich environments of *in vitro* buffers and biological systems alike, the extremely poor solubility of silver chloride results in very low (less than 1 ppb) equilibrium concentrations of free Ag(I) ions [20,21], and bacterial toxicity therefore relies on high potency or very high local Ag(I) concentration at the site of dissolution. As the concentration and rate of Ag(I) release are critical to toxicity and bactericidal efficacy, the ability to easily monitor free Ag(I) over time is of great interest. Furthermore, the ability to monitor release of Ag(I) from consumer products is critical to maintaining levels that are safe to humans and do not lead to the rapid development of resistance to silver by bacteria.

Traditional instrument methods for measuring silver include inductively coupled plasma-mass spectrometry and -optical emission spectrometry (ICP-MS and ICP-OES, respectively), flame and graphite furnace atomic absorption spectrometry (FAAS and GFAAS), and voltammetry [22,23]. These techniques have some restrictions, including interference at low analyte concentrations, and require sample preparation or digestion and complex instruments and trained operators. Importantly, these techniques lack the ability to differentiate between metallic silver, precipitated silver salts and complexes and free Ag(I). In general, for metal-sensing applications, optical detection approaches using selective sensors have been shown to be simple and cost-effective, with sensitivity to oxidation state and coordination environment [24,25]. Fluorescent probes should therefore provide an avenue for efficient monitoring of biologically relevant Ag(I) species at low concentrations.

Recent efforts to prepare fluorescent sensors for Ag(I) have included systems based on gold nanoparticles [26], carbon dots [27,28] and polyoxy-derivatized perylenediimide [29]. More traditional metal-sensing systems, involving a silver-selective receptor coupled to a fluorophore [30], have used a range of donor atoms for the soft Ag(I), from hard nitrogen and oxygen donors [31] to the very soft tellurium [32]. In sensing Ag(I), there is a particular challenge in achieving selectivity over other metal ions, with the main interferents being iron and copper [33,34], and mercury [35,36]. One approach to overcoming this interference is to seek spectral distinction of two similar ions, as has previously been achieved for an aggregation-induced emission sensor that responds to both silver and mercury [36].

Our interest is in developing sensors for monitoring the release of Ag(I) from silver-containing nanomaterials. For time-based studies we were particularly interested in identifying reversible sensors, which could sense not only increases in Ag(I) concentration but also respond to subsequent decreases in Ag(I) concentration. We have previously observed that sulfur-rich receptors designed for the sensing of Cu(I) showed some response to Ag(I) [37], and we have therefore been interested in using sulfur donor groups for the detection of silver. In this present study, we investigated thiocoumarin compounds, which have been reported as reaction-based mercury probes [38]. The response of the thiocoumarins to Hg(II), and to a lesser extent to Au(III) [39], occurs via desulfurization of the thiocarbonyl (figure 1*a*) to a carbonyl, yielding the brightly fluorescent oxo-coumarin derivative (figure 1*b*, coumarin 6). Other investigated metals ions did not catalyse this reaction, but notably the authors reported the appearance of a longer-wavelength peak upon addition of Ag(I). We therefore sought to investigate whether the thiocoumarin compound reported by Choi and co-workers [39], which we will refer to as **TcAg1** (figure 1*a*), could act as a silver sensor via an orthogonal signalling mechanism to the reported Hg(II)-catalysed desulfurization.

2. Experimental methods

2.1. General experimental methods

All solvents used were laboratory grade and were used without further purification unless otherwise stated. Milli-Q water was used to prepare all aqueous solutions. Reagents were purchased from Sigma Aldrich, Alfa Aesar and Combi-blocks. Analytical thin layer chromatography was performed on commercially prepared silica plates (Merck Kieselgel 60, 0.25 mm F_{254}). Flash column chromatography was performed using Davisil 230–400 mesh Kieselgel 60 silica eluting with solvents as described. Commercial materials were used as received unless otherwise noted.

2.2. Instrumentation

^{1}H NMR spectra were recorded at 298 K using a Bruker Avance III 400. ^{13}C NMR spectra were recorded on the same spectrometer at a frequency of 101 MHz. NMR data are referenced to residual solvent signal and processed using Topspin (Bruker). Chemical shifts (δ) are expressed in parts per million (ppm). Abbreviations used to describe NMR spectra are: s (singlet), d (doublet), t (triplet), q (quartet), m (multiplet) and/or br (broad). Mass spectrometry was performed on a Bruker AmaZon SL ion trap mass spectrometer.

ICP-MS measurements were performed using a Perkin Elmer Nexion 300X. Samples were digested in conc. HNO_3 overnight at room temperature before dilution with Milli-Q water to a 1 $\mu g\,l^{-1}$ to 1 $mg\,l^{-1}$ (i.e. 1 ppb – 1 ppm) concentration range. Calibration curves were constructed with Ag as a mixed standard using a Hamilton autodiluter. Internal standards Sc, Rh and Ir were infused inline via a mixing block with all samples and standards. All elements were measured in standard mode.

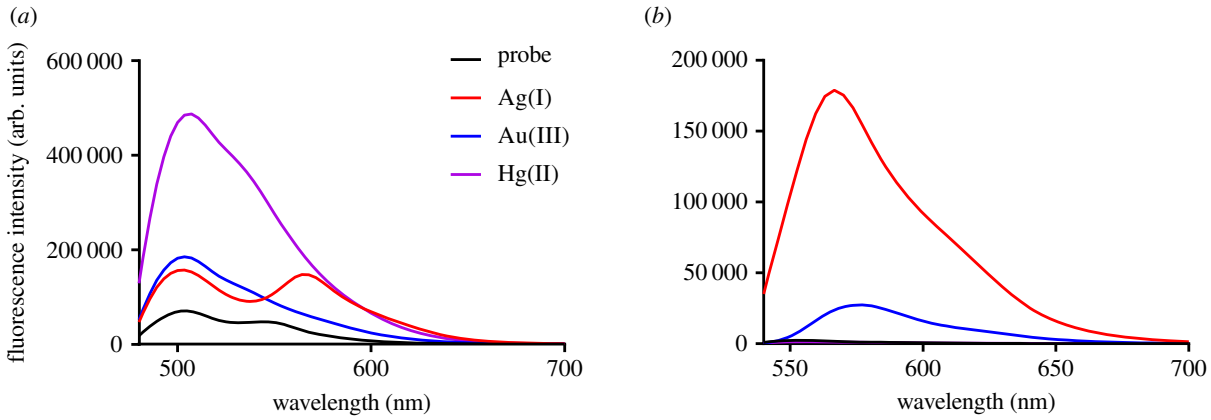

Figure 2. Fluorescence emission spectra of **TcAg1**; (*a*) 100 µM in THF, $\lambda_{ex} = 470$ nm, with 10 eq. of metal ion; (*b*) 100 µM in THF, $\lambda_{ex} = 530$ nm, with 10 eq. of metal.

Fluorescence measurements were performed on a PerkinElmer Enspire Plate Reader or a CaryEclipse 4000 fluorometer. pH studies were performed using 20 mM MES buffer (pH 5.5–6) and 20 mM chloride-free HEPES buffer (pH 7–9). Binding affinity was calculated using BindFit v. 0.5 (supramolecular.org).

2.3. Preparation of Ag(I)-doped phosphate-based glasses (AgPBGs)

AgPBGs were produced using NaH_2PO_4 (BDH, ≥98%), P_2O_5 (Sigma, ≥97%) and $CaCO_3$ (BDH, ≥98.5%). For the preparation of silver-containing PBGs, Ag_2SO_4 (Sigma, 99.99%) was also used. The required amount of each reagent was weighed and added to a fused silica crucible. The crucible was then placed in a preheated furnace at 1100°C for 1 h, after which the molten glass was poured into graphite moulds, which had been preheated to 350°C. The glass samples were allowed to cool to room temperature, and the resulting glass rods cut into discs by using a rotary diamond saw (Testbourne Ltd, Basingstoke, UK).

2.4. Inhibition of microbial growth by silver-doped phosphate-based glasses

AgPBGs (1 and 5 mol % Ag) were investigated for their ability to inhibit microbial growth using a disc diffusion methodology (BSAC Disc Diffusion Method for Antimicrobial Susceptibility Testing, Version 4, 2005). Iso-sensitest agar (Oxoid, Basingstoke, UK) plates were inoculated with a standardized culture of *Staphylococcus aureus* (NCTC 6571), *Escherichia coli* (NCTC 10418) and *Candida albicans* (NCPF 3179). Columbia agar (Oxoid, Basingstoke, UK) with 2% NaCl plates were inoculated with MRSA-16. In the case of the anaerobic bacterium *Clostridium difficile*, Wilkins-Chalgren agar plates supplemented with 5% horse blood (E & O Laboratories, UK) were used. AgPBGs discs of 5 mm diameter and 2 mm thickness were then placed on the inoculated plates. Discs not containing any silver were used as negative controls. These plates were then incubated overnight in air at 37°C. The diameters of any zones that had formed around the discs were measured in triplicate using calipers.

2.5. Effect of silver concentration on planktonic *Staphylococcus aureus*, *Escherichia coli* and *Candida albicans* growth

Staphylococcus aureus, *E. coli* and *C. albicans* cells were inoculated into 10 ml of nutrient broth and incubated overnight at 37°C with 200 r.p.m. agitation in an orbital shaker (Stuart Scientific, UK). The overnight cultures were used to inoculate a 5 ml volume of phosphate-buffered saline (PBS; Oxoid) to a standardized optical density of 0.03 at a wavelength of 600 nm (OD_{600}). AgPBGs discs of 12 mm diameter and 1 mm thickness were added to each tube, with the silver-free disc used as a control. The tubes were then incubated at 37°C. At various time intervals (up to 120 h) aliquots were removed and turbidity measurements were conducted at 600 nm. At each time interval serial dilutions of the suspensions were carried out in PBS. Fifty microlitres of the suspension and each dilution was spread onto MacConkey agar (Oxoid, Basingstoke, UK) plates. The plates were then incubated aerobically at 30°C for 48 h. For each type of disc, viable counts (colony forming units; CFUs) were conducted in triplicate.

2.6. Studies of Ag-doped phosphate glass

Discs of phosphate glass (15 mm diameter; 2 mm thickness) were placed in plastic specimen tubes. Each tube was filled with 50 ml of deionized water (pH 7 ± 0.5) or PBS saline solution (0.01 M, pH 7.4) and placed in a circulating water bath at 20°C or 37°C. At various time points (1, 6, 24, 48, 72, 96 and 120 h), a 250 µl aliquot of solution was removed and diluted with 240 µl of THF, before 10 µl of **TCAg1** stock solution in THF was added (10 µM final concentration of **TCAg1**) and a fluorescence measurement was taken. At each time point the phosphate glass samples were taken out of their respective containers and excess moisture was removed by blotting the samples dry with tissue before they were weighed. All the phosphate glass samples were returned into the same solution placed back into the water bath.

2.7. Synthetic methods

Compounds coumarin 6 [38], **TCAg1** [38] and 3-(2-benzoxazolyl)-7-(diethylamino)-2*H*-1-benzopyran-2-one [40] were prepared according to literature procedures (see electronic supplementary material, scheme S1).

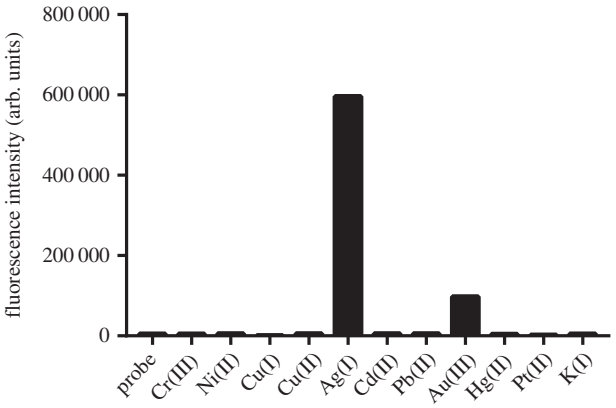

Figure 3. Fluorescence emission intensity of TCAg1 (100 μM) in the presence of metal ions (1 mM). Experiments performed in THF, $\lambda_{ex} = 530$ nm, $\lambda_{em} = 565$ nm.

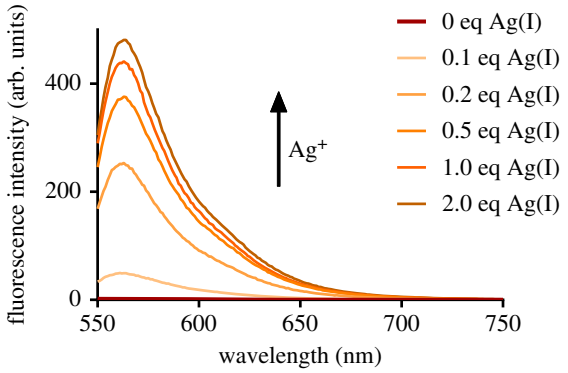

Figure 4. Fluorescence spectra of **TcAg1** with increasing concentrations of Ag(I) (10 μM probe, 1 : 1 THF/H_2O, $\lambda_{ex} = 530$ nm).

2.7.1. 3-(2-Benzoxazolyl)-7-(diethylamino)-*2H*-1-benzopyran-2-one (TCAgO)

To a solution of 3-(2-benzoxazolyl)-7-(diethylamino)-*2H*-1-benzopyran-2-one (28.3 mg, 0.085 mmol) in degassed toluene (15 ml) was added Lawesson's reagent (530 mg, 1.31 mmol). The orange mixture was heated at reflux for 3 days, under a nitrogen atmosphere. The red mixture was removed from the heat and allowed to cool to room temperature. The solvent was removed under reduced pressure to give a red oil which was purified by flash column chromatography (SiO_2; 2% methanol in dichloromethane) to afford **TCAgO** (22 mg, 73%) as a red oil. $R_f = 0.39$ (2% methanol in dichloromethane); ^{1}H NMR (400 MHz, $CDCl_3$) δ 8.27 (s, 1H), 7.84–7.78 (m, 1H), 7.63–7.58 (m, 1H), 7.42 (d, $J =$ 8.7 Hz, 1H), 7.38–7.33 (m, 2H), 6.73–6.65 (m, 2H), 3.47 (q, $J = 7.2$ Hz, 4H), 1.25 (t, $J = 7.2$ Hz, 6H) ppm; ^{13}C NMR (101 MHz, $CDCl_3$) δ 192.0, 152.9, 150.6, 141.7, 139.8, 130.4, 125.2, 124.4, 120.2, 119.8, 111.1, 110.7, 110.3, 96.6, 45.3, 12.5 ppm; HRMS ESI $[C_{20}H_{19}N_2O_2S]^+$ requires: 351.11618, found: 351.11622.

3. Results and discussion

3.1. Spectroscopic studies

When we treated **TcAg1** with $AgNO_3$ and excited at 470 nm, two emission peaks were observed at 511 nm and 565 nm (figure 2*a*). The shorter wavelength peak corresponds to the coumarin, which is a product of desulfurization, and the longer wavelength peak was envisaged to be due to non-covalent association of Ag(I). The excitation maximum for this Ag(I) responsive peak was 530 nm. Upon excitation at this wavelength, **TcAg1** showed minimal response in the absence of metal, or when treated with Hg(II) or a range of other metal ions (figures 2*b* and 3). Fluorescence titrations revealed a binding affinity for Ag(I) of 9.1×10^4M (electronic supplementary material, figure S1) and a limit of detection of 0.13 μM (electronic supplementary material, figure S2). This limit of detection is comparable to that documented in previous studies of fluorescent silver sensors, which typically report values between 5 nM and 5 μM [27,41–45].

To ensure practical application of the probe to environmental or medical uses, it was important that the probe function in an aqueous medium. With our interest in monitoring release of silver from nanomaterials, we did not require operation in 100% aqueous systems, and instead performed all subsequent experiments in a 1 : 1 aqueous and organic solvent mixture. Addition of increasing amounts of silver led to increasing intensity of the emission peak at 565 nm (figure 4), but monitoring the 511 nm emission peak (with excitation at 470 nm) revealed negligible formation of the carbonyl derivative upon silver addition (electronic supplementary material, figure S3). The effect of pH on **TcAg1** response to Ag(I) was assessed using non-complexing buffer solutions [46,47]. The fluorescence response remained consistent over the range of pH 6 to pH 8 (electronic supplementary material, figure S4). At higher pH values, a precipitate, presumed to be Ag_2O, was observed.

We then investigated the reversibility of the interaction of **TcAg1** with Ag(I). In 1 : 1 THF/H_2O, the probe could be converted from 'on' to 'off' via precipitation of silver with chloride or complexation of the silver with organic thiol-bearing ligands (figure 5*a*). This process could be cycled (figure 5*b*), although with less than 100% return of fluorescence with each cycle due to accumulation of a small but detectable amount of desulfurized product. This result highlights the difference in response of **TcAg1** to Ag(I) and Hg(II), with the latter causing an irreversible fluorescence change. We therefore sought to further understand the nature of the specific interaction between **TcAg1** and Ag(I).

3.2. Investigation of binding mode

Job's analysis did not show a standard profile with a single maximum (electronic supplementary material, figure S5a), instead indicating more complex coordination equilibria in solution, with maxima observed for both the 2 : 1 and 1 : 1 complexes. However, examination of titration data between 0 and 3 equivalents of Ag(I) shows a clear slope change at 1 equivalent, consistent with the predominance of a 1 : 1 complex (electronic supplementary material, figure S5b). The coordination of Ag(I) to the benzothiazole moiety, probably through the nitrogen, was expected to restrict the rotation of the benzothiazole, increasing the planarity of the conjugated system to result in the longer wavelength emission. We postulated the importance of both sulfur atoms in this coordination: direct coordination to the thioketone on the coumarin scaffold, and increasing the basicity of the nitrogen of the benzothiazole ring. To test this hypothesis, we

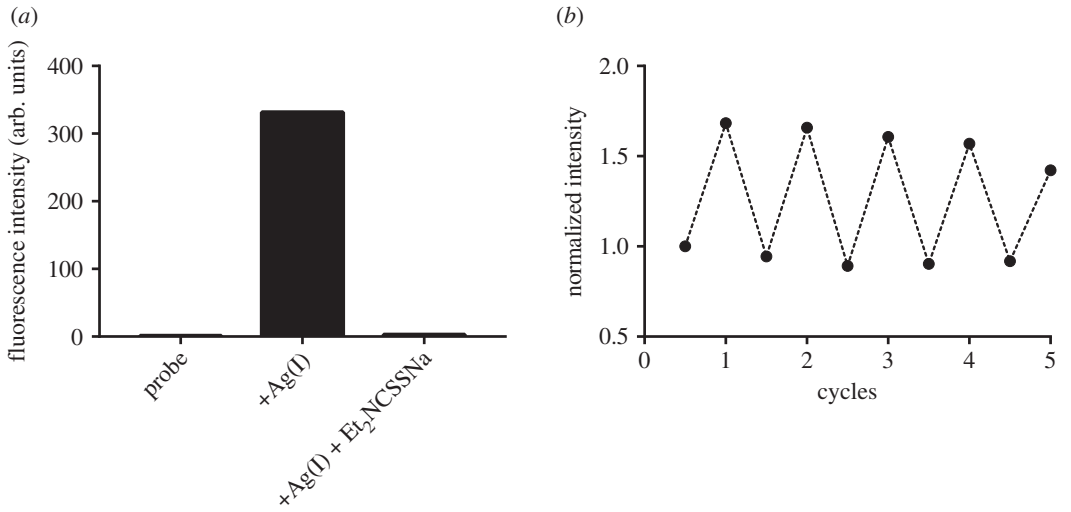

Figure 5. Reversibility studies of **TcAg1**; (*a*) 10 µM **TcAg1** and subsequent addition of $AgNO_3$ (5 eq.) and diethyldithiocarbamate (10 eq.) in 1 : 1 THF/H_2O; (*b*) conditions as per (*a*) with alternate additions of Ag(I) and diethyldithiocarbamate. $\lambda_{ex} = 530$ nm, $\lambda_{em} = 565$ nm. Emission values were normalized to the emission peak observed for $\lambda_{ex} = 470$ nm, $\lambda_{em} = 510$ nm.

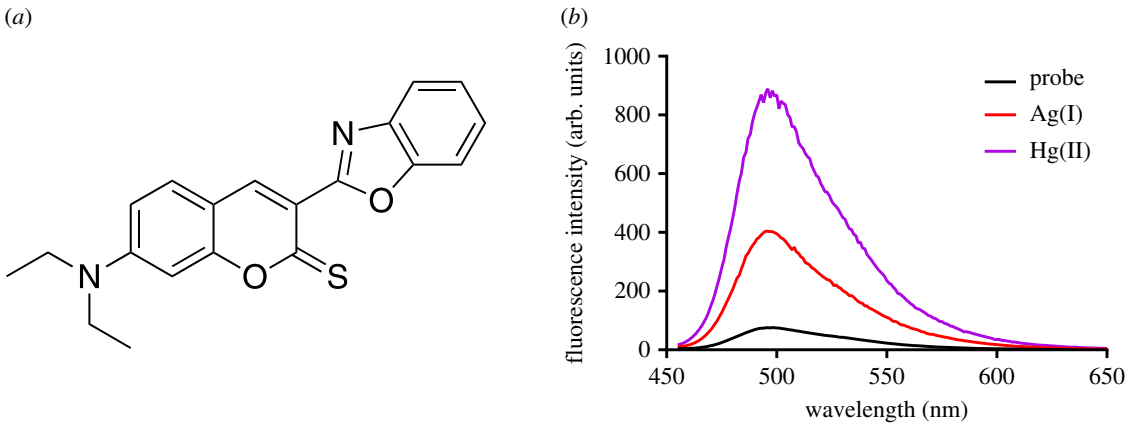

Figure 6. (*a*) Structure of **TCAgO**; (*b*) fluorescence spectrum of **TCAgO** (10 µM, 1:1 THF/H_2O, $\lambda_{ex} = 450$ nm, 10 eq. of metal ion).

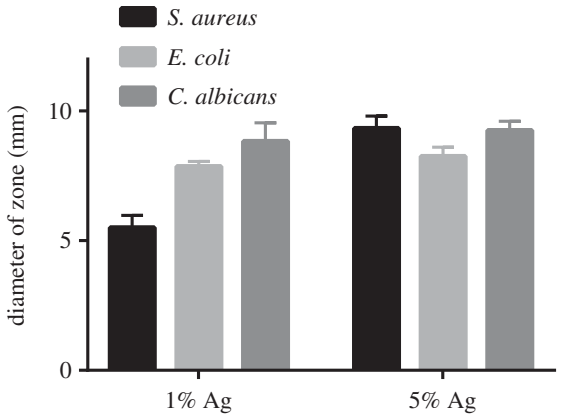

Figure 7. Disc diffusion assay conducted on 1 or 5 mol% Ag(I)-doped PBGs against *S. aureus*, *E. coli* and *C. albicans*. Error bars represent the standard deviation ($n = 3$).

synthesized the benzoxazole derivative **TCAgO** (figure 6*a*) in which the thiazolyl sulfur was replaced with an oxygen. Titration studies showed similar spectral profiles when either Ag(I) or Hg(II) were added, consistent with desulfurization in both cases. No additional emission peak was observed upon silver addition, suggesting no non-covalent interactions with Ag(I) such as that observed for **TcAg1** (figure 6*b*). We also investigated the effect of silver addition to coumarin 6, in which the thiocarbonyl sulfur is replaced with oxygen (figure 1*b*). Added Ag(I) did not give rise to a new fluorescence peak (electronic supplementary material, figure S3). We can therefore conclude that both sulfur atoms are required for the Ag(I)-binding interaction.

3.3. Silver-doped phosphate glass as a model silver-releasing agent

Having demonstrated that **TcAg1** responds reversibly to Ag(I), we were interested in investigating its ability to monitor Ag(I) release from silver-doped phosphate glass. Phosphate-based glasses, which are broadly used in medical applications [48], as well as silver nanoparticles [49], are of considerable interest in combating bacterial biofilm-related infections. In aqueous solutions, phosphate-based glasses dissolve over time and are considered bioresorbable and biocompatible [50], offering a method for the controlled release of Ag(I) [51]. Preliminary work has shown that while effective, the antibacterial efficacy of the glass does not vary relative to the silver content of the phosphate glass [52]. A better understanding of silver-containing functional

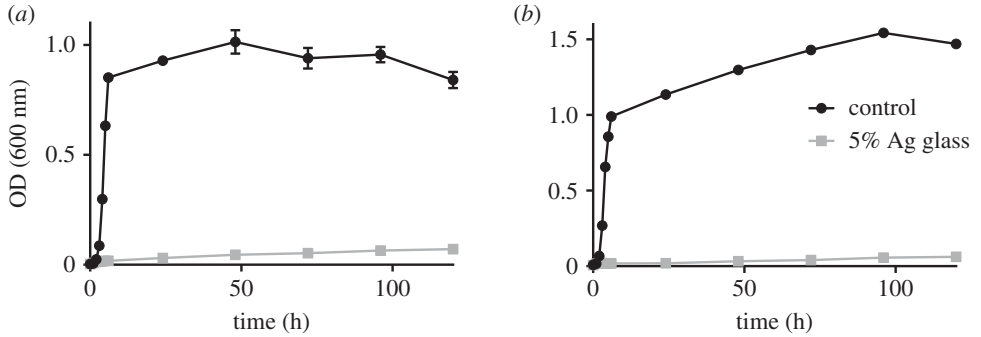

Figure 8. Optical density (turbidity) measurements of (*a*) *S. aureus* and (*b*) *E. coli* over 120 h in the absence and presence of 5% Ag-doped phosphate glass. Error bars represent the standard deviation ($n = 3$); for some data points error bars are too small to observe.

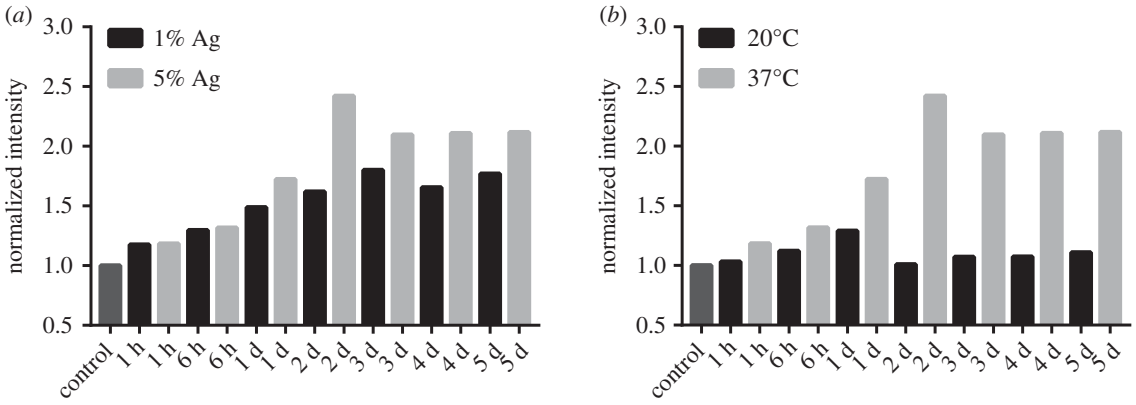

Figure 9. (*a*) One per cent or 5% Ag-doped phosphate glass incubated at 37°C with 10 µM **TcAg1** at each time point sampled in 1 : 1 THF/H_2O; (*b*) 5% Ag glass incubated at 20°C or 37°C in distilled H_2O, with 10 µM probe treatment at each time point, sampled in 1 : 1 THF/H_2O. Control is H_2O with no Ag-doped glass, 1 h, 37°C.

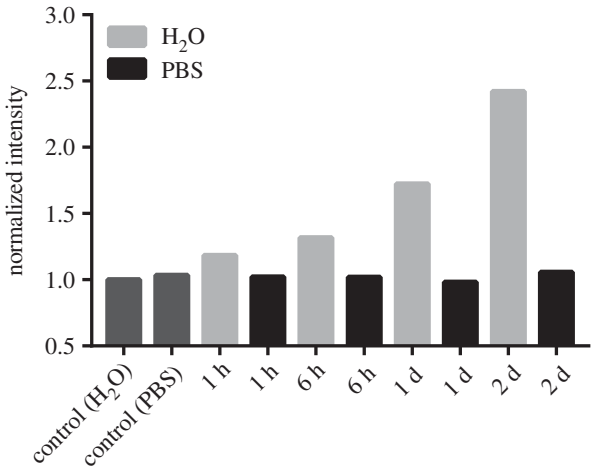

Figure 10. Five per cent Ag-doped phosphate glass incubated at 37°C with 10 µM **TcAg1** at each time point sampled in 1 : 1 THF/H_2O or 1 : 1 THF/PBS. Control is without Ag-doped glass, 1 h, 37°C.

materials is required for improving their implementation and in developing novel approaches to using these materials to treat or prevent harmful biofilms.

To generate a system on which to test the Ag-sensing ability of **TcAg1**, we prepared two glasses from 50 mol% P_2O_5, 30 mol% CaO, 1 or 5 mol% Ag_2O and the remainder Na_2O. The glasses were prepared by the conventional melt-quenching process, and the melted glass was cast into 12 mm cylinders in a preheated graphite mould placed in an annealing furnace at the required temperature.

The bactericidal activity of the glasses was tested using a disc diffusion assay. Glass discs (2 mm) were prepared from the cylinders and placed onto agar that had been inoculated with a bacterial or yeast strain. After 24 h, the diameter of free agar (bearing no bacteria/yeast) around the disc was measured as the zone of inhibition (figure 7). Both low and high silver-content glasses showed considerable ability to kill both Gram-positive (*S. aureus, MRSA, B. cereus*) and Gram-negative (*E. coli*, *pseudomonas*) bacteria, as well as pathogenic yeast (*C. albicans*). The 5% Ag-content glass showed slightly higher activity against all strains, and subsequent biological studies were therefore performed with this glass.

The bactericidal activity of the 5%-doped glass was further assessed by incubating suspensions of *S. aureus* and *E. coli* with glass discs and measuring the turbidity of the culture as a measure of bacterial density (figure 8). While control tubes showed the expected exponential and maintenance growth phases, there was very little increase in the turbidity of tubes containing a phosphate glass disc, confirming the high antibacterial activity of the phosphate glass. This was further confirmed when aliquots of the suspension were grown out on agar and colonies counted daily over the subsequent 5 days. Suspensions treated with the phosphate glass showed far fewer colonies than control suspensions at all time points (electronic supplementary material, figure S6).

3.4. Measurements of Ag(I) release from silver-doped phosphate glass

Having demonstrated the antibacterial and antifungal activity of the silver phosphate glasses, we sought to measure Ag(I) release over time using **TcAg1**. We incubated the two Ag(I)-doped phosphate glass in distilled water over the course of 5 days at

temperatures of 20°C and 37°C. Aliquots were periodically taken and tested using **TcAg1**, and the phosphate glass sample dried and weighed at the same time points. As expected, the 5% Ag-doped glass resulted in a higher fluorescence response at each time point compared to the 1% Ag-containing glass (figure 9*a*). Similarly, when comparing 5% Ag glass at 20°C versus 37°C, the increased temperature resulted in a higher fluorescence response (figure 9*b*), correlating to an increased phosphate glass dissolution rate and subsequent increased Ag(I) ion release. In each case, the fluorescence response increased up to 2 days before plateauing, although the phosphate glass continued to dissolve, evidenced by the continued decreasing mass of the dried sample (electronic supplementary material, figure S7) and the increasing total Ag(I) content of the solution as measured by ICP-MS (electronic supplementary material, figure S8). This was attributed to the limit of available Ag(I) species in solution, which is the parameter measured by **TcAg1**. By contrast, ICP-MS measurements, which report on total silver content, whether free Ag(I), insoluble silver salts or complexed silver ions, show a consistent increase in total silver release over 5 days (electronic supplementary material, figure S8).

These observations were further emphasized when the Ag-doped phosphate glass was incubated in PBS (figure 10). No turn-on of **TcAg1** was observed at any time point, although the phosphate glass mass decreased over time at a comparable rate to that observed in the distilled water incubation. In PBS, it is expected that released Ag(I) would be precipitated as chloride or phosphate salts, precluding any Ag(I) interaction with **TcAg1**. These results demonstrate that **TcAg1** has utility in specifically reporting on free Ag(I) ions rather than total Ag release, and therefore provides a valuable complementary method to traditionally employed techniques for measuring bulk silver.

4. Conclusion

As the toxicity of silver—whether to bacteria, aquatic life or humans—is highly dependent on its speciation, it is clear that alternatives are needed to traditional methods that report on bulk silver levels. Importantly, too, these new methods must be sensitive to the low levels of labile Ag(I) expected in environmental samples. With a sub-micromolar detection limit and a micromolar binding affinity, we have been able to confirm that **TcAg1** is well suited to this role.

In the present study, we have used **TcAg1** to study the release of silver from Ag-doped phosphate glass, just one of the many commonly used silver-containing nanomaterials that could be investigated with this system. With the added advantage of reversibility of response, **TcAg1** could also be used in the future to study the fluctuations in silver levels over time, for example in environmental samples. Immobilization of the probe onto solid surfaces would further assist in this aim. More widespread use of this probe could provide insights into the inconsistencies in the bactericidal efficacy of silver materials, and aid in developing better practice in the use of these materials.

Data accessibility. All raw data and sample materials are stored at the University of Sydney and are accessible upon request.

Authors' contributions. Z.L. performed synthesis and studies of phosphate glasses, participated in data analysis and drafted the manuscript. D.G.S. participated in the design of the study, and performed synthesis and spectroscopic studies. J.L.K. performed synthesis and spectroscopic studies. R.L.M. performed synthesis and spectroscopic studies. J.C.K. participated in design of the phosphate glass and coordinated the testing. S.-Y.B. prepared the phosphate glass and performed microbial studies. W.C. participated in the design of the study, performed microbial analysis of the phosphate glass and helped draft the manuscript. E.J.N. designed and coordinated the study and helped draft the manuscript. All the authors gave their final approval for publication.

Competing interests. We have no competing interests.

Funding. This project has received funding from the Australian Research Council (DP150100649) and the European Union's Horizon 2020 research and innovation programme, under grant agreement number 739572. S.-Y.B. acknowledges the financial support of the EPSRC for an industrial CASE award grant reference EP/M507970/1.

Acknowledgements. The authors would like to acknowledge the Westpac Bicentennial Foundation for a Research Fellowship (E.J.N.), the University of Sydney for SOAR Fellowships (W.C. and E.J.N.), a Henry Bertie and Florence Mabel Gritton Postdoctoral Research Fellowship (D.G.S.), and the Australian government for a Research Training Program Scholarship (R.L.M.). We acknowledge the scientific and technical assistance of the Australian Microscopy and Microanalysis Research Facility at the Australian Centre for Microscopy and Microanalysis (ACMM).

References

1. Huang G-W, Xiao H-M, Fu S-Y. 2014 Paper-based silver-nanowire electronic circuits with outstanding electrical conductivity and extreme bending stability. *Nanoscale* **6**, 8495–8502. (doi:10.1039/C4NR00846D)
2. Chen W, Liu Y, Courtney HS, Bettenga M, Agrawal CM, Bumgardner JD, Ong JL. 2006 *In vitro* anti-bacterial and biological properties of magnetron co-sputtered silver-containing hydroxyapatite coating. *Biomaterials* **27**, 5512–5517. (doi:10.1016/j.biomaterials.2006.07.003)
3. Gilchrist T, Healy DM, Drake C. 1991 Controlled silver-releasing polymers and their potential for urinary tract infection control. *Biomaterials* **12**, 76–78. (doi:10.1016/0142-9612(91)90136-X)
4. Hong KH. 2007 Preparation and properties of electrospun poly(vinyl alcohol)/silver fiber web as wound dressings. *Polym. Eng. Sci.* **47**, 43–49. (doi:10.1002/pen.20660)
5. Maki DG. 2010 *In vitro* studies of a novel antimicrobial luer-activated needleless connector for prevention of catheter-related bloodstream infection. *Clin. Infect. Dis.* **50**, 1580–1587. (doi:10.1086/652764)
6. Wahid F, Zhong C, Wang HS, Hu XH, Chu LQ. 2017 Recent advances in antimicrobial hydrogels containing metal ions and metals/metal oxide nanoparticles. *Polymers* **9**, 636. (doi:10.3390/polym9120636)
7. Siddiqi KS, Husen A, Rao RAK. 2018 A review on biosynthesis of silver nanoparticles and their biocidal properties. *J. Nanobiotechnol.* **16**, 14. (doi:10.1186/s12951-018-0334-5)
8. Zhao JY, Zhong D, Zhou SB. 2018 NIR-I-to-NIR-II fluorescent nanomaterials for biomedical imaging and cancer therapy. *J. Biomed. Mater. Res. B Appl. Biomater.* **6**, 349–365. (doi:10.1039/C7TB02573D)
9. Zhang Q, Yang MY, Zhu Y, Mao CB. 2018 Metallic nanoclusters for cancer imaging and therapy. *Curr. Med. Chem.* **25**, 1379–1396. (doi:10.2174/0929867324666170331122757)
10. Pugazhendhi A, Edison T, Karuppusamy I, Kathirvel B. 2018 Inorganic nanoparticles: a potential cancer therapy for human welfare. *Int. J. Pharm.* **539**, 104–111. (doi:10.1016/j.ijpharm.2018.01.034)
11. Faya M, Kalhapure RS, Kumalo HM, Waddad AY, Omolo C, Govender T. 2018 Conjugates and nano-delivery of antimicrobial peptides for enhancing therapeutic activity. *J. Drug Deliv. Sci. Technol.* **44**, 153–171. (doi:10.1016/j.jddst.2017.12.010)
12. Arce Funck J, Danger M, Gismondi E, Cossu-Leguille C, Guérold F, Felten V. 2013 Behavioural and physiological responses of *Gammarus fossarum* (Crustacea Amphipoda) exposed to silver. *Aquat.*

Toxicol. **142–143**, 73–84. (doi:10.1016/j.aquatox.2013.07.012)

13. Hogstrand C, Wood CM. 1998 Toward a better understanding of the bioavailability, physiology, and toxicity of silver in fish: implications for water quality criteria. *Environ. Toxicol. Chem.* **17**, 547–561. (doi:10.1002/etc.5620170405)
14. McGillicuddy E *et al.* 2017 Silver nanoparticles in the environment: sources, detection and ecotoxicology. *Sci. Total Environ.* **575**, 231–246. (doi:10.1016/j.scitotenv.2016.10.041)
15. Ratte HT. 1999 Bioaccumulation and toxicity of silver compounds: a review. *Environ. Toxicol. Chem.* **18**, 89–108. (doi:10.1002/etc.5620180112)
16. Adams NWH, Kramer JR. 1998 Reactivity of Ag^{+} ion with thiol ligands in the presence of iron sulfide. *Environ. Toxicol. Chem.* **17**, 625–629. (doi:10.1002/etc.5620170415)
17. Gorsuch JW, Klaine SJ. 1998 Toxicity and fate of silver in the environment. *Environ. Toxicol. Chem.* **17**, 537–538.
18. Shafer MM, Overdier JT, Armstong DE. 1998 Removal, partitioning, and fate of silver and other metals in wastewater treatment plants and effluent-receiving streams. *Environ. Toxicol. Chem.* **17**, 630–641. (doi:10.1002/etc.5620170416)
19. Xiu Z-M, Zhang Q-B, Puppala HL, Colvin VL, Alvarez PJJ. 2012 Negligible particle-specific antibacterial activity of silver nanoparticles. *Nano Lett.* **12**, 4271–4275. (doi:10.1021/nl301934w)
20. Loza K, Diendorf J, Sengstock C, Ruiz-Gonzalez L, Gonzalez-Calbet JM, Vallet-Regi M, Köller M, Epple M. 2014 The dissolution and biological effects of silver nanoparticles in biological media. *J. Biomed. Mater. Res. B Appl. Biomater.* **2**, 1634–1643. (doi:10.1039/c3tb21569e)
21. Kaiser J-P, Roesslein M, Diener L, Wichser A, Nowack B, Wick P. 2017 Cytotoxic effects of nanosilver are highly dependent on the chloride concentration and the presence of organic compounds in the cell culture media. *J. Nanobiotechnol.* **15**, 5. (doi:10.1186/s12951-016-0244-3)
22. Barriada JL, Tappin AD, Evans EH, Achterberg EP. 2007 Dissolved silver measurements in seawater. *TrAC Trends Anal. Chem.* **26**, 809–817. (doi:10.1016/j.trac.2007.06.004)
23. Howe PD, Dobson S. 2002 *Silver and silver compounds: environmental aspects*. Geneva, Switzerland: World Health Organisation.
24. Kolanowski JL, Dawson LJ, Mitchell L, Lim Z, Graziotto ME, Filipek WK, Hambley TW, New EJ. 2018 A fluorescent probe for investigating metabolic stability of active transplatin analogues. *Sens. Actuators B* **255**, 2721–2724. (doi:10.1016/j.snb.2017.09.084)
25. New EJ. 2016 Harnessing the potential of small molecule intracellular fluorescent sensors. *ACS Sens.* **1**, 328–333. (doi:10.1021/acssensors.6b00148)
26. Xiao ZY, Tang AJ, Huang HS, Wang Z. 2017 A simple and sensitive sensor for silver ions based on unmodified gold nanoparticles by using dynamic light scattering techniques. *Can. J. Chem.* **95**, 1267–1272. (doi:10.1139/cjc-2017-0241)
27. Tabaraki R, Nateghi A. 2016 Nitrogen-doped graphene quantum dots: 'turn-off' fluorescent probe for detection of Ag^{+} Ions. *J. Fluoresc.* **26**, 297–305. (doi:10.1007/s10895-015-1714-y)
28. Liu GL, Xuan CL, Feng DQ, Hua DL, Liu TH, Qi G, Wang W. 2017 Dual-modal fluorescence and light-scattering sensor based on water-soluble carbon dots for silver ions detection. *Anal. Methods* **9**, 5611–5617. (doi:10.1039/C7AY01873H)
29. Ongun MZ, Ertekin K, Nadeem S, Birel O. 2016 Polyoxy-derivatized perylenediimide as selective fluorescent Ag (I) chemosensor. *J. Fluoresc.* **26**, 2311–2320. (doi:10.1007/s10895-016-1927-8)
30. Kaur A, Lim Z, Yang K, New EJ. 2016 Fluorescent sensors for biological metal ions. In *Comprehensive supramolecular chemistry II* (ed. T Glass), pp. 295–317. Amsterdam, Netherlands: Elsevier.
31. Li Z, Ou-Yang J, Fu Y-J, Li C-Y, Li Y-F, Li S-J. 2017 A borondipyrrolemethene-based turn-on fluorescent probe for silver ion with high sensitivity and selectivity and its application in water samples and living cells. *Tetrahedron Lett.* **58**, 3536–3540. (doi:10.1016/j.tetlet.2017.07.092)
32. Bhasin AKK, Singh J, Singh H, Raj P, Singh N, Kaur N, Bhasin KK. 2017 A novel approach to explore organochalcogen chemistry of tellurium based receptor for selective determination of silver ions in aqueous medium. *Polyhedron* **125**(Suppl. C), 238–245. (doi:10.1016/j.poly.2016.11.048)
33. Bhorge YR, Chou TL, Chen YZ, Yen YP. 2015 New coumarin-based dual chromogenic probe: naked eye detection of copper and silver ions. *Sens. Actuator B* **220**, 1139–1144. (doi:10.1016/j.snb.2015.06.059)
34. Hammud HH, El Shazly S, Sonji G, Sonji N, Bouhadir KH. 2015 Thiophene aldehyde-diamino uracil Schiff base: a novel fluorescent probe for detection and quantification of cupric, silver and ferric ions. *Spectrochim. Acta A Mol. Biomol. Spectrosc.* **150**, 94–103. (doi:10.1016/j.saa.2015.05.038)
35. Ye J-H, Duan L, Yan C, Zhang W, He W. 2012 A new ratiometric Ag^{+} fluorescent sensor based on aggregation-induced emission. *Tetrahedron Lett.* **53**, 593–596. (doi:10.1016/j.tetlet.2011.11.107)
36. Chen S, Wang WJ, Yan MM, Tu Q, Chen SW, Li TB, Yuan MS, Wang J. 2018 2-Hydroxy benzothiazole modified rhodol: aggregation-induced emission and dual-channel fluorescence sensing of Hg^{2+} and Ag^{+} ions. *Sens. Actuator B* **255**, 2086–2094. (doi:10.1016/j.snb.2017.09.008)
37. Shen C, Kolanowski JL, Tran CMN, Kaur A, Akerfeldt MC, Rahme MS, Hambley TW, New EJ. 2016 A ratiometric fluorescent sensor for the mitochondrial copper pool. *Metallomics* **8**, 915–919. (doi:10.1039/C6MT00083E)
38. Choi MG, Kim YH, Namgoong JE, Chang S-K. 2009 Hg^{2+}-selective chromogenic and fluorogenic chemodosimeter based on thiocoumarins. *Chem. Commun.* **2009**, 3560–3562. (doi:10.1039/b905612b)
39. Park JE, Choi MG, Chang S-K. 2012 Colorimetric and fluorescent signaling of Au^{3+} by desulfurization of thiocoumarin. *Inorg. Chem.* **51**, 2880–2884. (doi:10.1021/ic202080v)
40. Ye F-F, Gao J-R, Sheng W-J, Jia J-H. 2008 One-pot synthesis of coumarin derivatives. *Dyes Pigm.* **77**, 556–558. (doi:10.1016/j.dyepig.2007.08.005)
41. Liao S, Zhao XY, Zhu FW, Chen MA, Wu ZL, Song XZ, Yang H, Chen X. 2018 Novel S, N-doped carbon quantum dot-based 'off-on' fluorescent sensor for silver ion and cysteine. *Talanta* **180**, 300–308. (doi:10.1016/j.talanta.2017.12.040)
42. Zhang CL, Han Z, Wang MJ, Yang ZH, Ran XQ, He WJ. 2018 A new BODIPY-derived ratiometric senor with internal charge transfer (ICT) effect: colorimetric/fluorometric sensing of Ag^{+}. *Dalton Trans.* **47**, 2285–2291. (doi:10.1039/C7DT04345G)
43. Kaewanan P, Sricharoen P, Limchoowong N, Sripakdee T, Nuengmatcha P, Chanthai S. 2017 A fluorescence switching sensor based on graphene quantum dots decorated with Hg^{2+} and hydrolyzed thioacetamide for highly Ag^{+}-sensitive and selective detection. *RSC Adv.* **7**, 48 058–48 067. (doi:10.1039/C7RA09126E)
44. Cayuela A, Soriano ML, Kennedy SR, Steed JW, Valcarcel M. 2016 Fluorescent carbon quantum dot hydrogels for direct determination of silver ions. *Talanta* **151**, 100–105. (doi:10.1016/j.talanta.2016.01.029)
45. Yang Y, Li WY, Qi H, Zhang QF, Chen J, Wang Y, Wang B, Wang S, Yu C. 2012 Detection of silver(I) ions based on the controlled self-assembly of a perylene fluorescence probe. *Anal. Biochem.* **430**, 48–52. (doi:10.1016/j.ab.2012.07.024)
46. Ferreira CMH, Pinto ISS, Soares EV, Soares HMVM. 2015 (Un)suitability of the use of pH buffers in biological, biochemical and environmental studies and their interaction with metal ions—a review. *RSC Adv.* **5**, 30 989–31 003. (doi:10.1039/C4RA15453C)
47. Good NE, Winget GD, Winter W, Connolly TN, Izawa S, Singh RMM. 1966 Hydrogen ion buffers for biological research. *Biochemistry* **5**, 467–477. (doi:10.1021/bi00866a011)
48. Knowles JC. 2003 Phosphate based glasses for biomedical applications. *J. Mater. Chem.* **13**, 2395–2401. (doi:10.1039/b307119g)
49. Ikuma K, Decho AW, Lau BL. 2015 When nanoparticles meet biofilms—interactions guiding the environmental fate and accumulation of nanoparticles. *Front. Microbiol.* **6**, 591. (doi:10.3389/fmicb.2015.00591)
50. Moss RM, Pickup DM, Ahmed I, Knowles JC, Smith ME, Newport RJ. 2008 Structural characteristics of antibacterial bioresorbable phosphate glass. *Adv. Funct. Mater.* **18**, 634–639. (doi:10.1002/adfm.200700721)
51. Valappil SP, Pickup DM, Carroll DL, Hope CK, Pratten J, Newport RJ, Smith ME, Wilson M, Knowles JC. 2007 Effect of silver content on the structure and antibacterial activity of silver-doped phosphate-based glasses. *Antimicrob. Agents Chemother.* **51**, 4453–4461. (doi:10.1128/AAC.00605-07)
52. Valappil SP, Knowles JC, Wilson M. 2008 Effect of silver-doped phosphate-based glasses on bacterial biofilm growth. *Appl. Environ. Microbiol.* **74**, 5228–5230. (doi:10.1128/AEM.00086-08)